

NONLINEAR OPTICAL PHENOMENA

PACS numbers: 42.55.Rz; 42.70.Hj; 42.70.Mp
DOI: 10.1070/QE2015v045n06ABEH015687

Absorption spectra and nonlinear transmission (at λ = 2940 nm) of a diffusion-doped Fe^{2+}:ZnSe single crystal

G.A. Bufetova, E.S. Gulyamova, N.N. Il'ichev, A.S. Nasibov, P.P. Pashinin, P.V. Shapkin

Abstract. **Transmission spectra of a ZnSe sample diffusion-doped with Fe^{2+} ions have been measured in the wavelength range 500–7000 nm. A broad absorption band in the range 500–1500 nm has been observed in both doped and undoped regions of the sample. This band is possibly due to deviations from stoichiometry in the course of diffusion doping. The transmission of the Fe^{2+}:ZnSe sample at a wavelength of 2940 nm has been measured at various dopant concentrations and high peak pulse intensities (up to 8 MW cm^{-2}). The samples have been shown to be incompletely bleached: during a laser pulse, the transmission first increases, reaches a maximum, and then falls off. Our results suggest that the incomplete bleaching cannot be accounted for by excited-state absorption. The incomplete bleaching (as well as the transmission maximum) is due to the heating of the sample, which leads to a reduction in upper level lifetime and, accordingly, to an increase in absorption saturation intensity.**

Keywords: *ZnSe crystal, diffusion doping, absorption spectra, nonlinear transmission.*

1. Introduction

One promising material for high-power solid-state lasers operating in the wavelength range 4000–5000 nm is Fe^{2+}-doped ZnSe. Adams et al. [1] studied its absorption and luminescence spectra and obtained lasing in the wavelength range 4000–4500 nm at temperatures below 180 K. Kernal et al. [2] demonstrated room-temperature lasing of this material. Il'ichev et al. [3] reported room-temperature superluminescence of a diffusion-doped Fe^{2+}:ZnSe crystal pumped by a 2940-nm laser. Using transverse pumping of a Fe^{2+}:ZnSe crystal by a HF laser, Velikanov et al. [4] obtained a laser pulse energy of 30.6 mJ.

Mirov et al. [5] presented a review of results on Fe^{2+}-doped chalcogenide crystals. An important feature of Fe^{2+}:ZnSe is that the Fe^{2+} upper laser level lifetime is a strong function of temperature [1, 6, 7]. It is worth noting that lifetime assessment from the luminescence decay rate at room temperature or above presents some difficulties because of the low luminescence quantum yield. In particular, the Fe^{2+} upper laser level lifetime in ZnSe crystals drops from 105 μs at 120 K [1] to 355 ns at 300 K [6]. Upper laser level lifetimes measured in the range 275–365 K were reported by Frolov et al. [8].

As shown by measuring the linear and nonlinear transmission of a Fe^{2+}:ZnSe crystal at a wavelength of 2940 nm and temperatures from 20 to 220 °C [9], there is essentially no bleaching at an incident intensity of ~5.5 MW cm^{-2} and a temperature of 220 °C. This leads us to conclude that the Fe^{2+} upper laser level lifetime at a temperature of 220 °C is shorter than 12 ns.

Transmission measurements for a diffusion-doped Fe^{2+}:ZnSe crystal at a high power of 2920-nm radiation confirmed incomplete bleaching of the crystal, i.e. it had residual losses [10]. The experimental data were shown to be better described at an Fe^{2+} upper laser level lifetime of 100 ns. Diffusion doping of ZnSe single crystals with Fe^{2+} ions was discussed in Refs [11, 12]. Il'ichev et al. [12] measured the temperature-dependent diffusion coefficient of Fe^{2+} ions in a zinc selenide single crystal.

Since high-power laser radiation causes incomplete bleaching of ZnSe samples diffusion-doped with Fe^{2+}, the question arises whether or not this is related to the doping procedure, because in the case of diffusion doping the dopant is distributed very nonuniformly over the sample, which may influence the degree of bleaching of the material, for example, if there is concentration quenching of luminescence.

The objectives of this work were to measure spectral characteristics of a ZnSe sample diffusion-doped with Fe^{2+} and investigate nonlinear transmission of high-power laser radiation at a wavelength of 2940 nm through the sample.

2. Measurement of transmission spectra

We measured the transmission spectrum of a diffusion-doped Fe^{2+}:ZnSe single crystal (sample 435). Diffusion was carried out through two opposite faces of the crystal, which had the form of a plane-parallel plate. After the diffusion process, both faces of the sample had Fe-rich layers. Next, a layer ~500 μm in thickness was cut away on one side, and the newly exposed surface was polished to optical quality. The opposite face was cut away at an angle of about 3° and also polished. The dimensions of the polished face were 10.5 × 16 mm, and the thickness of the sample varied from 2.8 to 2.0 mm over a length of 16 mm. As a result, no Fe was detected optically at one end of the sample, whereas the other end had the maximum Fe concentration. Transmission spectra were measured on Shimadzu IR-460 and UV-3101PC spectrophotometers. To measure the spectra, an identical optical wedge was made from undoped ZnSe. The two samples were placed

G.A. Bufetova, E.S. Gulyamova, N.N. Il'ichev, P.P. Pashinin
A.M. Prokhorov General Physics Institute, Russian Academy of Sciences, ul. Vavilova 38, 119991 Moscow, Russia;
e-mail: ilichev@kapella.gpi.ru;
A.S. Nasibov P.N. Lebedev Physics Institute, Russian Academy of Sciences, Leninsky prosp. 53, 119991 Moscow, Russia

Received 2 October 2014; revision received 14 November 2014
Kvantovaya Elektronika **45** (6) 521–526 (2015)
Translated by O.M. Tsarev

so that there was no angular beam deviation in the spectral instrument.

Figure 1 shows the transmission spectrum of a plane-parallel ZnSe plate and two transmission spectra of the Fe^{2+}:ZnSe sample, normalised to the transmission spectrum of the undoped ZnSe plate. The normalisation excludes the reflection from the faces of the additional optical wedge. Spectra (*1*) in Fig. 1 correspond to regions of the samples that contain little or no Fe^{2+}, so the absorption line of Fe^{2+} near 3000 nm is missing in these spectra. In spectra (*2*), the absorption line of Fe^{2+} near 3000 nm is seen, because the beam passes through that part of the sample which contains Fe^{2+} ions. It is worth noting that the spectra were obtained with different instruments and in different regions of the sample, so spectra (*2*) in Fig. 1 differ from each other.

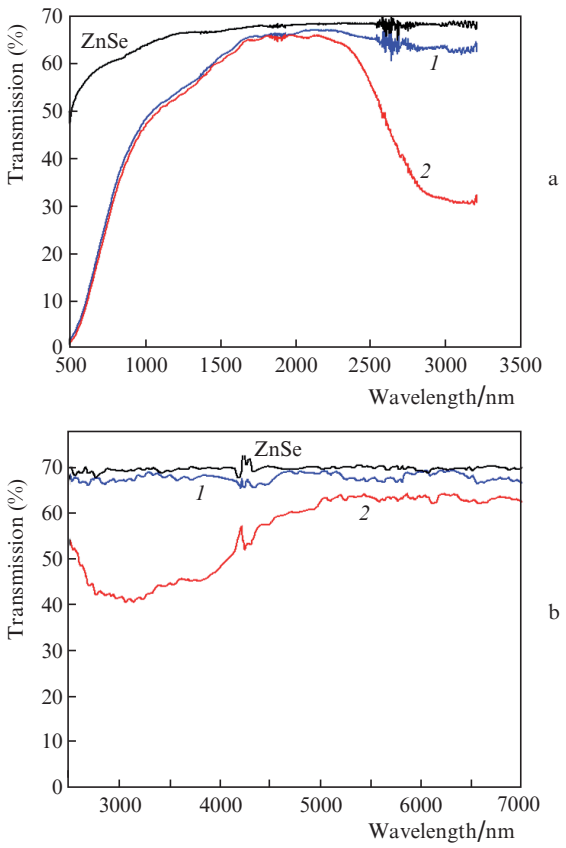

Figure 1. Transmission spectra of the Fe^{2+}:ZnSe sample in regions (*1*) free of and (*2*) containing Fe^{2+} and spectra of a plane-parallel ZnSe plate in the ranges (a) 500–3200 and (b) 2500–7000 nm.

Note also that an important feature of the above transmission spectra of Fe^{2+}:ZnSe is the broad absorption band in the range 500–1500 nm, which is present in both the Fe^{2+}-doped and undoped regions of the crystal. Clearly, it originated from the doping process. It may be that the spectral range in question contains as well an absorption line of Fe, which is however obscured by the broad absorption band.

3. Setup for nonlinear transmission measurements

The population of the Fe^{2+} upper level in a ZnSe crystal exposed to high-power laser radiation is determined by the probability of its decay in unit time, the power of the radiation absorbed on the resonance transition and other processes that may result from interaction between high-power radiation and a given impurity centre. Therefore, the transmission dynamics during a laser pulse can be used to evaluate the decay time in question. This approach to lifetime assessment is of particular interest for centres that have a low luminescence quantum yield.

Figure 2 shows a schematic diagram of the experiment. To measure transmission as a function of time, we used two FSG-22-3a2 photodetectors, one of which (reference) served to detect the radiation incident on the sample, and the other (measuring) detected the radiation transmitted through the sample. Electrical signals were measured with a Tektronix DPO 7254 2.5-GHz oscilloscope (input resistance of the oscilloscope, 50 Ω; time resolution of the photodetectors at a load of 50 Ω, about 2.5 ns). The output of an actively *Q*-switched pulsed Er:YAG laser having a near-TEM_{00} transverse beam profile was focused into the sample (*6*) by a lens (*5*). The laser wavelength was 2940 nm, the pulse duration was about 220 ns, the cross-sectional area of the Gaussian beam on the sample surface was 1.06×10^{-3} cm^2 (radius of 0.026 cm), the pulse energy was about 2.3 mJ, and the peak energy density was 2.16 J cm^{-2}. The plane of the sample coincided with the focal plane of a CaF_2 lens with a focal length $f_1 = 150$ mm (*7*). Some distance from it, there was another CaF_2 lens, with a focal length $f_2 = 300$ mm (*9*). In the focal plane of the latter lens was located a radiation diffuser (*11*) made from 14 frosted GGG crystal plates 450 μm in thickness and 5 mm in diameter, placed sequentially in a copper tube with a polished inner surface. The diffuser was placed immediately in front of the input window of the photodetector and was intended to fill the active area of the photoresistor with radiation and reduce the impact of beam spot displacement in the input plane of the diffuser on the photodetector signal. The aperture of lenses *7* and *9* was 80 mm. An NS9 glass filter (*8*) was placed between the lenses and attenuated the beam by approx-

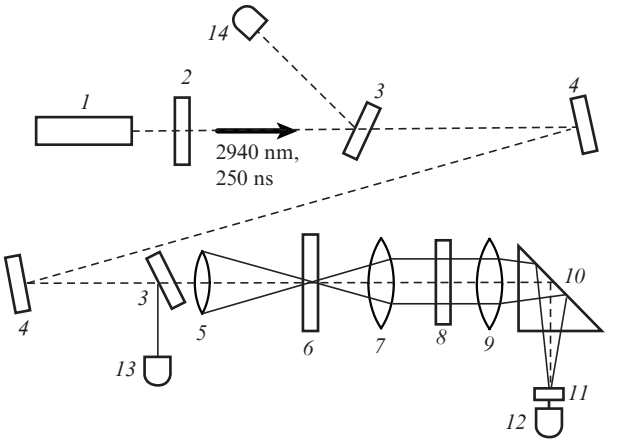

Figure 2. Schematic of the setup for transmission measurements: (*1*) Er:YAG laser; (*2*) attenuating filter; (*3*) quartz glass substrates; (*4*) folding metallic flat mirrors; (*5*) $f = 700$ mm CaF_2 lens focusing the beam onto the sample; (*6*) ZnSe or Fe^{2+}:ZnSe sample (near-normal incidence); (*7*) $f = 150$ mm CaF_2 lens (with the sample in its focal plane); (*8*) NS9 attenuating filter; (*9*) $f = 300$ mm CaF_2 lens; (*10*) folding CaF_2 prism; (*11*) diffuser; (*12*) FSG-22-3a2 signal photodetector; (*13*) FSG-22-3a2 reference photodetector; (*14*) PM4 photodetector for pulse energy measurements.

imately 200 times. A CaF_2 prism was used to change the beam direction by 90°.

Transmission measurements were made for both high-power and attenuated radiation. In the case of high-power radiation, filter *8* was placed between lenses *7* and *9*; in the case of weak pulses, it was placed in front of the sample. The use of two lenses was necessary because high-power radiation heated the sample, producing a thermal lens with a time-dependent focal length. The two-lens scheme made it possible to preclude the possible effect of thermal lensing on the shape of the electrical signal in detecting the radiation transmitted through the sample, and the large aperture of the lenses prevented vignetting of the transmitted beam. Possible beam vignetting on the aperture of the detector was also ruled out by using the diffuser described above. In addition, the wedge changed the beam direction. Since the output plane of the crystal was imaged by the optical system on the input plane of the diffuser, the position of the image of the transmitted beam was insensitive to the presence of the sample, as ascertained in separate experiments.

4. Signal measurement and processing

The transmission measurement procedure was as follows. The signals from photodetectors *13* and *12* (Fig. 2) were measured in two channels of the oscilloscope (Fig. 2). The signal U from the photoresistance, which was detected together with its dc component, was transformed as

$$u_x = \frac{U/U_p}{1 - U/U_p},$$

were U_p is the power supply voltage. From this signal, we subtracted its dc component u_{xt}, which was determined at an instant in time far from the signal maximum: $u = u_x - u_{xt}$. It is this transformed signal that was subsequently analysed. The signal from the measuring photodetector, $u_1(t)$, was divided by that from the reference photodetector, $u_0(t)$, at each instant in time t in the range chosen. The time delay between the instant when the signals arrived at the oscilloscope channels and the instant when the beam arrived at the sample was nearly zero. If the $u_1(t)/u_0(t)$ ratio is $r_0(t)$ when the measuring channel contains no sample and $r_1(t)$ when the sample is present in the measuring channel, the transmission of the sample is given by $T(t) = r_1(t)/r_0(t)$. Time $t = 0$ corresponded to the pulse peak. The $U(t)$ signal was determined as the average over 16 pulses. The oscilloscope was triggered at a fixed level near half the amplitude of the average signal from the reference photodetector. The pulse distortion on averaging on account of the signal amplitude instability at a fixed triggering level can be neglected, because the distortion is not large according to mathematical modelling.

The transmission of sample 435 was measured in regions differing in dopant concentration. The beam was incident on that side of the sample where the dopant concentration was low (Fig. 3). The transmission was measured at different positions of the sample in the transverse direction (along the y axis). In this measurement procedure, a layer of the material with some dopant concentration, which depends on x-coordinate, is added for each subsequent position of the sample with respect to the preceding one. Here, the wedge is thought of as a combination of steps.

If the measured transmission of layer $[0, x_1]$ for position y_1 is T_1 and that of layer $[0, x_2]$ for position y_2 is T_2, the transmission of layer $[x_1, x_2]$, of thickness $\Delta x = x_2 - x_1$, is $T_{12} = T_2/T_1$. The intensity on the input surface of layer $[x_1, x_2]$ is equal to that at the output surface of layer $[0, x_1]$ if the intensity at the input surface of the sample is maintained constant. The thicknesses of the layers were evaluated from the known displacement of the sample along the y axis and the wedge angle.

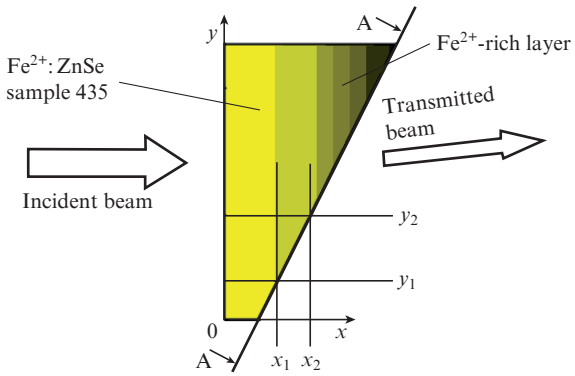

Figure 3. Schematic illustrating beam propagation through sample 435. The A–A plane is imaged on the input plane of the diffuser.

5. Results of the nonlinear transmission measurements

Figure 4 shows time dependences of the 100% transmission line (with no sample) for a weak (w) (peak intensity of 0.04 MW cm^{-2}) and a strong (s) (peak intensity of 8 MW cm^{-2}) field. It is seen that this line deviates from the 100% level by no more than 1% during the entire pulse. Also presented in Fig. 4 are the time dependences of transmission for the undoped ZnSe optical wedge. It follows from these data that the strong-signal transmission of the wedge is T_s = 67% (ZnSes curve) and its weak-signal transmission is T_w = 68% (ZnSew curve), and that the transmission is constant during a laser pulse to an accuracy of better than 0.5%. The relative error in our transmission measurements within the pulse

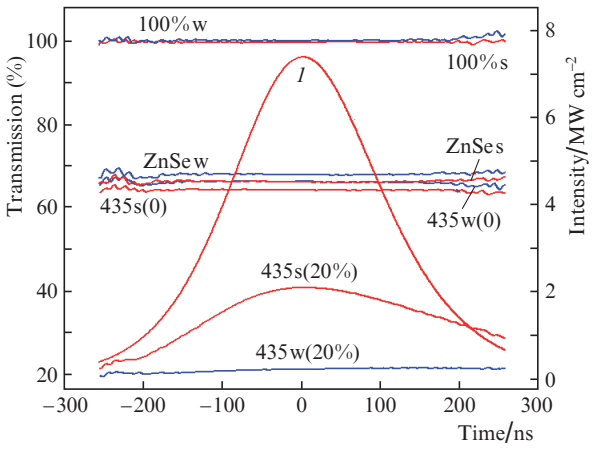

Figure 4. Time dependences of transmission for the undoped ZnSe wedge and the Fe^{2+}:ZnSe sample 435 in a Fe^{2+}-free region [435w, s(0)] and in a region where the initial transmission is about 20% [435w, s(20%) and ZnSew, s(20%)] and 100% transmission curves (with no sample) for a weak and a strong field; (*1*) time dependence of the intensity on the input surface of the sample.

duration was estimated at 1%. The calculated transmission of the plane-parallel ZnSe plate is about 68%, which is due to the reflection from the faces of the sample (refractive index of 2.43 at wavelengths near 3 μm [13]) and agrees with the transmission of the plate measured on a spectrophotometer at a wavelength of 2940 nm (Fig. 1a).

In addition, Fig. 4 shows the transmission of an undoped region of the Fe^{2+}:ZnSe sample 435 [curves 435s(0) and 435w(0)]. It is seen that the transmission is essentially time-independent (T_s = 64% in the strong field and T_w = 66% in the weak field). Comparison of these curves with the transmission curves of the wedge (T_s = 66.3% and T_w = 68%) leads us to conclude that they are identical and differ only in the transmission value, which is, most likely, caused by inaccurate adjustment of the system. The samples probably have a nonresonant absorption at a wavelength of 2940 nm, but the accuracy in our measurements allows us to estimate only the upper limit of the nonresonant absorption coefficient: $\gamma < 0.5\ \mathrm{cm}^{-1}$.

Curves 435s(20%) and 435w(20%) in Fig. 4 represent the strong- and weak-field transmission of the sample in the presence of Fe^{2+} (20%). In the strong field, the transmission increases during the first half of the pulse and decreases during the second half. Characteristically, there is a transmission maximum at an instant in time near the maximum intensity of the laser pulse incident on the sample. In the weak field, the transmission is essentially constant during the entire pulse. Also presented in Fig. 4 is the time dependence of the beam intensity on the input surface of the sample.

In data processing, the intensity on the input and output surfaces of the sample was reduced to that in the sample. Absolute intensity values were used to find the saturation intensity and estimate the irradiation-induced change in the temperature of the sample.

Figure 5 shows the time dependences of transmission for the individual layers described above (see Section 4). It is seen that, in all our measurements in the weak field, the transmission is constant during a laser pulse to an accuracy of better than 1%. In the case of intense radiation, the transmission curves of all the layers have a characteristic shape: the transmission increases after the beginning of a laser pulse and reaches a maximum, before falling off after the pulse peak.

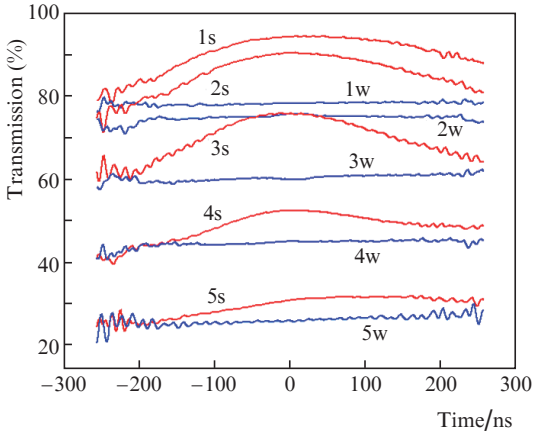

Figure 5. Time dependences of transmission for individual layers (1–5). The parameters of the layers are given in Table 1.

Table 1.

Layer	h/μm	T_w (%)	T_s^{max} (%)	γ_w/cm^{-1}	Temperature/°C
1	52	78	94.3	47	27
2	26	75	90	112	40
3	26	60	76	193	59
4	26	45	52	309	73
5	26	26	32	513	56

Table 1 gives the thicknesses of the layers (h), their weak-field transmission, peak strong-field transmission, average absorption coefficients, and calculated temperatures at the instant when their transmission passes through a maximum.

6. Discussion

One possible reason for the fact that the transmission at the pulse peak is substantially lower than 100% is excited-state absorption. This process can be characterised by the parameter $\beta = \ln T_s / \ln T_w$. At a sufficiently high incident intensity, it is equal to the ratio of the excited-state absorption cross section to the ground-state absorption cross section [14]. Clearly, β should be independent of dopant concentration. The data in Table 1 can be used to construct a graph of β against the absorption coefficient of a layer (Fig. 6). It is seen from the graph that β varies from 0.2 to 0.8. This wide range leads us to conclude that excited-state absorption cannot account for the incomplete bleaching of the sample in the strong field.

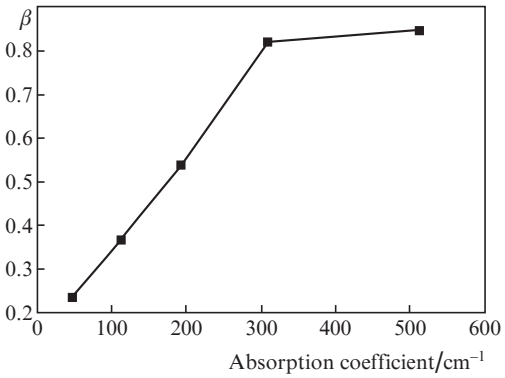

Figure 6. $\beta = \ln T_s / \ln T_w$ as a function of the average weak-field absorption coefficient of a layer.

The propagation of radiation of intensity I (photons cm^{-2} s^{-1}) through the sample and the time dependence of the concentration n_1 of Fe^{2+} on the lower level can be described by the rate equations

$$\frac{\mathrm{d}I}{\mathrm{d}x} = -\sigma_{12} n_1 I, \qquad \frac{\mathrm{d}n_1}{\mathrm{d}t} = -\sigma_{12} n_1 I + \frac{1}{\tau(x,t)}(n_0 - n_1), \tag{1}$$

where σ_{12} is the absorption cross section for the transition from the lower level 1 to the upper level 2; $\tau(x,t)$ is the upper level lifetime at point x and time t; and $n_0(x)$ is the dopant concentration at this point of the sample. We assume that there is no nonresonant absorption. From Eqns (1), we obtain the following equation for the time-dependent transmission of the sample:

$$\frac{1}{T}\frac{\mathrm{d}T}{\mathrm{d}t} = -I_{\mathrm{in}}\sigma_{12}(1-T) + \frac{1}{\bar{\tau}(t)}\ln\frac{T}{T_{\mathrm{w}}}. \qquad (2)$$

Here, $T = I_{\mathrm{out}}/I_{\mathrm{in}}$ is the transmission of the sample; I_{in} and I_{out} are the intensities on the input and output surfaces of the sample at the transverse distribution maximum;

$$T_{\mathrm{w}} = \exp\left[-\sigma_{12}\int_0^L n_0(x)\,\mathrm{d}x\right]$$

is the weak-field transmission of the sample; L is the beam path length in the sample; and $\bar{\tau}(x)$ is defined by the relation

$$\int_0^L \frac{n_0(x)-n_1(x)}{\tau(x,t)}\,\mathrm{d}x = \frac{1}{\bar{\tau}(t)}\int_0^L [n_0(x)-n_1(x)]\,\mathrm{d}x.$$

From (2), we can find the saturation intensity $I_{\mathrm{sat}} = \hbar\omega_{\mathrm{p}}\times(\tau\sigma_{12})^{-1}$ (W cm^{-2}) at time $t = t_{\max}$ when the transmission passes through a maximum, i.e. $[\mathrm{d}T/\mathrm{d}t]_{t=t_{\max}} = 0$:

$$I_{\mathrm{sat}} = \hbar\omega_{\mathrm{p}}\left[\frac{I_{\mathrm{in}}(1-T)}{\ln(T/T_{\mathrm{w}})}\right]_{t=t_{\max}}. \qquad (3)$$

Let us estimate the heating of the sample by high-power radiation. The energy deposited as heat in an individual layer, which is thought to have a constant dopant concentration throughout, can be found as the difference between the energy densities E_{in} and E_{out} at time $t = t_{\max}$. It is also necessary to take into account the energy stored by excited Fe^{2+} ions in the layer. Using (2) and neglecting the energy removal from the heating zone via luminescence, we obtain the change in the temperature of the layer at the instant when its transmission has a maximum:

$$\Delta T = \left[\frac{(E_{\mathrm{in}}-E_{\mathrm{out}}) - \hbar\omega_{\mathrm{lum}}\sigma_{12}^{-1}\ln(T/T_{\mathrm{w}})}{Ch\rho}\right]_{t=t_{\max}}, \qquad (4)$$

where $\hbar\omega_{\mathrm{lum}}$ is the photon energy of the Fe^{2+} luminescence; $\sigma_{12} = 0.95\times10^{-18}$ cm^2 [1] is the absorption cross section at a wavelength of 2940 nm; $C = 0.33$ J g^{-1} K^{-1} is the specific heat of ZnSe [15]; $\rho = 5.3$ g cm^{-3} [13]; and h is the thickness of the layer. E_{in} and E_{out} were determined experimentally. Table 1 presents the ΔT calculation results obtained using (4) (room temperature was taken to be 20 °C). The heat removal from the heating zone through heat conduction can be neglected, because the heat diffusion length $\Delta L = [\chi\Delta t/(C\rho)]^{1/2}$ over the pulse duration is about 1.5 μm, which is considerably smaller than the characteristic thickness of an individual layer (~20 μm). Here, $\chi = 0.19$ W cm^{-1} K^{-1} is the thermal conductivity of ZnSe [13] and $\Delta t = 220$ ns is the pulse duration.

In Fig. 7, the saturation intensity calculated using (3) and the data in Table 1 is shown as a function of the average absorption coefficient of a layer. Since $I_{\mathrm{sat}} \sim \tau^{-1}$, these data can be explained under the assumption that the upper level lifetime τ decreases with increasing dopant concentration (concentration quenching of luminescence). This possibility was pointed out previously [7]. At the same time, one should take into account the heating of the material by high-power radiation. Also shown in Fig. 7 is the temperature of the corresponding layer calculated using (4). It is seen that the heating is rather appreciable, especially where the dopant concentration is high. In particular, at an absorption coefficient near 300 cm^{-1}, the temperature at the laser pulse peak exceeds 70 °C. At this temperature, the upper level lifetime is considerably shorter [8]. Because of this, we assume that the concentration dependence of the saturation intensity in Fig. 7 results from the heating of the sample by the high-power radiation. Line (*1*) in Fig. 7 is a linear fit for the concentration dependence of the saturation intensity at a room-temperature saturation intensity $I_{\mathrm{sat}}(20\,^\circ\mathrm{C}) = 0.2$ MW cm^{-2} ($\tau \sim 355$ ns at 300 K [6]) and a nearly zero dopant concentration. The insufficient accuracy in our transmission measurements makes it impossible to find I_{sat} from experimental data. We can only indicate the range of possible saturation intensities: 0.1 MW cm^{-2} < $I_{\mathrm{sat}}(20\,^\circ\mathrm{C})$ < 1 MW cm^{-2}.

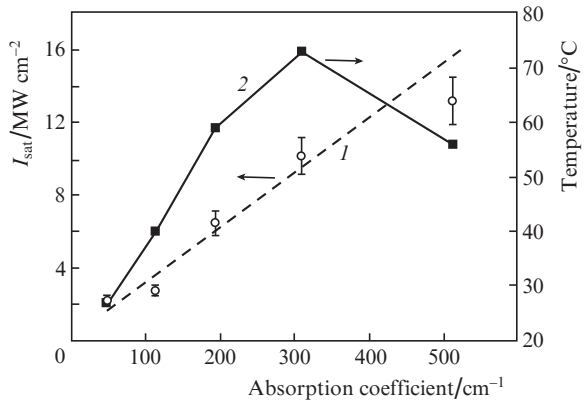

Figure 7. (*1*) Saturation intensity and (*2*) temperature of a layer as functions of the average absorption coefficient of the layer.

Returning to the strong-field transmission curves in Fig. 5 [curves (1s)–(4s)], note that the drop in transmission for $t > 0$ can be accounted for by the further heating of the sample and the associated reduction in the Fe^{2+} upper level lifetime.

7. Conclusions

1. Transmission spectra of a Fe^{2+}-doped ZnSe sample have been measured in the wavelength range 500–7000 nm. The sample was diffusion-doped at thermodynamic equilibrium. Using a wedge sample in which the Fe^{2+}-rich layer was cut away at an angle of 3°, we were able to perform measurements in several regions differing in dopant concentration. The broad absorption band in the range 500–1500 nm, present in diffusion-doped ZnSe samples, was also observed in Fe^{2+}-free regions of the crystal. This band is possibly due to changes in the stoichiometry of the crystal under the effect of the high-temperature in the diffusion process.

2. The transmission of the sample at high incident intensity (peak intensity of about 8 MW cm^{-2}) and a wavelength of 2940 nm has been measured during a laser pulse. The transmission has been shown to have a maximum near the laser pulse peak. After a 200-fold attenuation of the laser beam, the transmission of the sample was constant during a laser pulse.

3. The measurement results indicate that the incomplete bleaching of the sample cannot be accounted for by excited-state absorption.

4. We have measured the saturation intensity at a wavelength of 2940 nm (Fe^{2+} resonance transition) at the instant in time corresponding to the transmission maximum in regions differing in Fe^{2+} concentration. The saturation intensity has been shown to be a strong function of the average absorption

coefficient, which is due to the heating of the sample by the high-power radiation. An increase in the temperature of the sample leads to a reduction in Fe^{2+} upper level lifetime and, accordingly, to an increase in saturation intensity.

Acknowledgements. This work was supported in part by the Russian Foundation for Basic Research (Grant Nos 13-02-01073a, 12-02-00641a, 12-02-00465a and 13-02-12181 ofi-m) and the RF President's Grants Council (Support to the Leading Russian Scientific Schools Programme, Grant No. NSh-451.2014.2).

References

1. Adams J.J., Bibeau C., Page R.H., et al. *Opt. Lett*., **24** (23), 1720 (1999).
2. Kernal J., Fedorov V.V., Gallian A., et al. *Opt. Express*, **13** (26) 10608 (2005).
3. Il'ichev N.N., Danilov V.P., Kalinushkin V.P., et al. *Kvantovaya Elektron*., **38** (2), 95 (2008) [*Quantum Electron*., **38** (2), 95 (2008)].
4. Velikanov S.D., Danilov V.P., Zakharov N.G., et al. *Kvantovaya Elektron*., **44** (2), 141 (2014) [*Quantum Electron*., **44** (2), 141 (2014)].
5. Mirov S.B., Fedorov V.V., Martyshkin D.V., et al. *Opt. Mater. Express*, **1** (5), 898 (2011).
6. Akimov V.I., Voronov A.A., Kozlovskii V.I., et al. *Kvantovaya Elektron*., **36** (4), 299 (2006) [*Quantum Electron*., **36** (4), 299 (2006)].
7. Myoung NoSoung, Fedorov V.V., Mirov S.B. *Proc. SPIE Int. Soc. Opt. Eng*., **8588**, 85881H1 (2010).
8. Frolov M.P., Korostelin Yu.V., et al. *Laser Phys. Lett*., **10**, 125001 (2013).
9. Il'ichev N.N., Pashinin P.P., Gulyamova E.S., Bufetova G.A., Shapkin P.V., Nasibov A.S. *Kvantovaya Elektron*., **44** (3), 213 (2014) [*Quantum Electron*., **44** (3), 213 (2014)].
10. Il'ichev N.N., Shapkin P.V., Kulevsky L.A., Gulyamova E.S., Nasibov A.S. *Laser Phys*., **18** (2), 130 (2008).
11. Demirbas U., Sennaroglu A., Somer M. *Opt. Mater*., **28**, 231 (2006).
12. Il'ichev N.N., Shapkin P.V., Gulyamova E.S., Kulevsky L.A., Nasibov A.S. *Neorg. Mater*., **46** (2), 149 (2010).
13. Blistanov A.A., Bondarenko V.S., et al. *Akusticheskie kristally. Spravochnik* (Acoustic Crystals: A Handbook) (Moscow: Nauka, 1982).
14. Wei T.H., Hagau D.J., Sence M.J., et al. *Appl. Phys. B*, **54**, 46 (1992).
15. Bergman G.A., Gusarov A.V. http://www.chem.msu.su/Zn/Zn/print-ZnSe_c.html.